Journal of Materials Chemistry A

ROYAL SOCIETY OF CHEMISTRY

PAPER

View Article Online
View Journal

Cite this: DOI: 10.1039/d6ta02261h

Metallopolymers *via* thermal dealkylation of unstrained bisphosphanylferrocene precursors

Subhayan Dey, *[ab] Balázs Szathmári, [c] Dennis Langgut,[a] Torsten Gutmann,*[de] Zsolt Kelemen *[c] and Rudolf Pietschnig *[a]

Ferrocenylene-bridged polyphosphanes $[Fc'P_2]_n{}^tBu_2$ and $[Fc'P_2]_n$ (Fc′ = 1,1′-ferrocenediyl; ^{t}Bu = *tert*-butyl), previously prepared *via* thermal ring expansion polymerization from strained ferrocenophane precursors, are reported to be accessible from unstrained secondary phosphanes. The thermal reaction and polymerization of $Fe(C_5H_4\text{-}PH^tBu)_2$ proceed through the elimination of ^{t}BuH and consequent formation of ^{t}Bu-substituted diphospha[2]FCP, along with ferrocene substituted cyclic P_4-species and di-^{t}Bu-substituted linear P_4-species. The resulting polymer shows similar ^{13}C and ^{31}P solid-state NMR, IR, and UV-vis spectra and elemental analysis results, when compared to those of authentic samples of previously published $[Fc'P_2]_n{}^tBu_2$ and $[Fc'P_2]_n$ obtained *via* strained ferrocenophanes. In contrast, the thermal reaction of all-^{t}Bu-substituted tertiary phosphane $Fc'(P^tBu_2)_2$ entails loss of the P-containing moiety along with formation of Fc^{t}Bu instead of a polymeric material. Thermodynamic assessment of the decomposition pathways of both precursors based on density functional theory calculations is consistent with the experimental findings. Overall, the unstrained 1,1′-ferrocenylene bridged secondary bisphosphane provides a simplified approach for thermal polymerization to linear one-dimensional P_n-chains.

Received 16th March 2026
Accepted 7th May 2026

DOI: 10.1039/d6ta02261h

rsc.li/materials-a

1. Introduction

Inorganic polymers offer remarkable upgradation in properties (*e.g.* higher decomposition temperature, lower flammability, lower glass transition temperature, *etc.*) compared with organic polymers.[1] They frequently consist of a handful of main-group elements, such as P, N, B, S, Si, *etc.* (*e.g.* cyclo- and poly-phosphazenes and their polymers, polyborazines, poly-thiophosphazenes, polysilanes, polysiloxanes, *etc.*).[2,3] Similarly, polymers with organometallic moieties as sidechains (*i.e.* pendant polymer **A**, Fig. 1) or as part of the backbone (*i.e.* mainchain polymer **B**, Fig. 1) are especially attractive owing to their unique properties such as reversible redox properties in the case of ferrocene allowing for switchable or adaptive materials.[4,5]

While ferrocene-based sidechain polymers (**A**, Fig. 1) are commonly synthesized by polymerization of precursors with a polymerizable unit attached to ferrocene (*e.g.* the vinyl group),[4,6,7] main-chain polymers (**B**, Fig. 1) are commonly synthesized *via* directed ring-opening polymerization reactions (ROPs) of strained ferrocenophane (FCP) rings (**C**, Fig. 1),[8] where the dihedral angle α may be used to estimate the ring-strain in the molecule.[9,10]

Recently,[5,8] we have introduced a synthetic approach to oligo-/polymeric 1D-phosphorus chains **4** with ferrocenylene-bridges,[13] using ring expansion polymerization (REP) which employs thermal P–C dissociation and ring-opening of a di-phospha[2]FCP **2** (Scheme 1).[14] In the course of this REP sequence a tetracyclic tetraphosphane intermediate **3** could be identified (Scheme 1) which has been fully characterized upon preparation *via* an independent synthetic route using salt

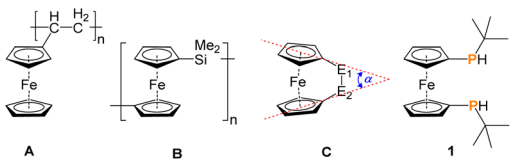

Fig. 1 Prominent examples of ferrocene containing sidechain (**A**)[11] and mainchain polymers (**B**).[12] General sketch of precursors, a strained ferrocenophane (E = organoelement fragment; α = dihedral or tilt angle) (**C**)[8] and unstrained 1,1′-disubstituted ferrocene bisphosphane (**1**) used in this work.

[a]*Institut für Chemie und CINSaT, University of Kassel, Heinrich-Plett-Straße 40, 34132 Kassel, Germany. E-mail: pietschnig@uni-kassel.de*

[b]*Department of Chemistry, School of Advanced Sciences, Vellore Institute of Technology, Vandalur-Kelambakkam Road, Keelakotaiyur, Chennai, Tamil Nadu 600127, India. E-mail: subhayan.dey@vit.ac.in*

[c]*Department of Inorganic and Analytical Chemistry, Faculty of Chemical Technology and Biotechnology, Budapest University of Technology and Economics, Műegyetem rkp 3, 1111, Budapest, Hungary. E-mail: kelemen.zsolt@vbk.bme.hu*

[d]*Department of Chemistry, Paderborn University, Warburger Str. 100, 33098 Paderborn, Germany. E-mail: torsten.gutmann@uni-paderborn.de*

[e]*Institute of Inorg. and Phys. Chemistry, TU Darmstadt, Peter-Grünberg-Str. 8, 64287 Darmstadt, Germany*

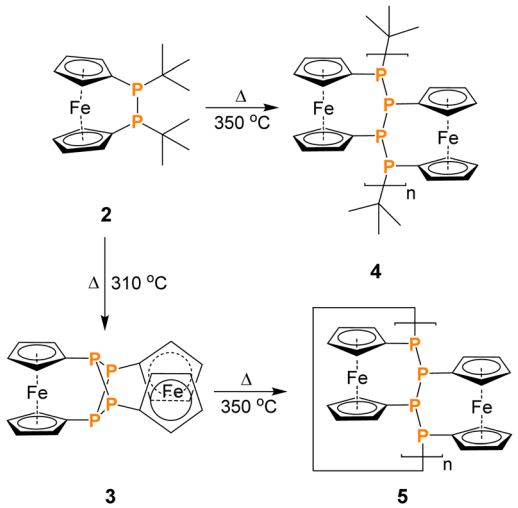

Scheme 1 Thermal ring-expansion polymerization of phospha[2]FCP (**2**), *via* formation of a tetracyclic tetraphosphane with twofold FCP bridges (**3**).

metathesis under mild conditions.[15] Consistent with its role as a central intermediate in the above mentioned REP, samples of isolated **3** are thermally transformed into a ferrocenylene-bridged polyphosphane metallopolymer (**5**) (Scheme 1).[15]

It is noteworthy that polymerization reactions *via* elimination of the small molecules have received significant attention. In particular, transition-metal catalyzed dehydrocoupling routes have been established for the preparation of polymers with inorganic backbones, such as Si–Si,[16] Ge–Ge,[17] Sn–Sn,[18] P–B,[19] and Si–O.[20] Catalytic dehydrocoupling involving pnictogens has been successfully utilized to access challenging products.[21–23] In this vein, dehydrocoupling reactions of primary phosphines received particular attention using heat (Scheme 2a),[24] or chemical reagents (*e.g.* $Cp^*_2SnCl_2$ (Scheme 2b),[25] N-heterocyclic carbenes, *etc.*[26]) to drive polymerization.[27] On the other hand, the dehydrocoupling of secondary phosphines has almost exclusively been achieved in the presence of transition metal catalysts for a few specific starting materials like phosphine boranes (Scheme 2c).[28–30] To the best of our knowledge,

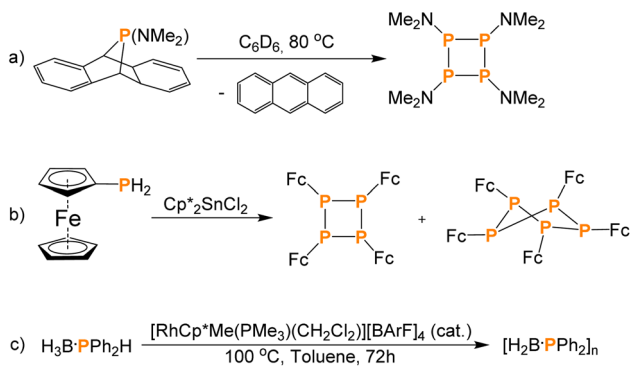

Scheme 2 Thermally (a)[24] or chemically driven (b)[25] and catalytic (c)[28] dehydropolymerization of primary and secondary phosphanes, where Fc stands for 1-ferrocenyl unit.

no precedence of thermal polymerization *via* dealkylation of secondary phosphines is available in the literature.

In light of facile thermal P–C and P–P activation, during REP employing moderate to low strained precursors,[13,15] we set out to investigate thermal reactions of their unstrained open-chain counterpart **1** using it as the starting material (Fig. 1). The thus-obtained solid materials have been compared with authentic samples of the previously reported polymers **4** and **5** including by solid-state NMR.[13,15] To obtain an insight into thermodynamic and mechanistic aspects of the polymerization, we employed density functional theory (DFT), for interpretation of the experimentally obtained results.

2. Results and discussion

The previously reported thermal cleavage of P–C and P–P bonds at elevated temperatures (*i.e.* 310 °C and 350 °C) on a moderately strained and a virtually unstrained [2]– and [3]FCP (**2** and **3**, respectively) inspired us to investigate the scope of a similar reaction on a truly unstrained secondary phosphane. Hydrogen and *tert*-butyl substituted **1** was chosen as a potentially suitable starting material, as it can be obtained *via* a well-established synthetic protocol as an air stable compound,[31] owing to the presence of the ferrocene unit.[32] For the combination of hydrogen and *tert*-butyl groups as substituents on the phosphanyl groups, formation of an easily removable volatile byproduct (such as *tert*-butane) can be anticipated. To explore the dissociative polymerization, compound **1** was placed under high vacuum in a sealed glass ampule and subsequently heated from room temperature to 250 °C with a step-wise increase by 10 °C retaining the conditions of each step unchanged for 1 h. After observing a prominent change in viscosity at *ca.* 240 °C, the reaction temperature was maintained at 250 °C for 4 h. Upon cooling the reaction ampule to room temperature, the semi-solid brown substance was extracted in C_6D_6, which upon investigation with liquid NMR spectroscopy showed a mixture of P–P coupled products besides unreacted **1** (doublet at δ −27.10 ppm), FcP^tBuH (singlet at δ −26.64 ppm), and ^{t}BuPH_2 (singlet at δ −80.31 ppm) (Scheme 3 and Fig. 2). The P–P coupled products have been identified as diphospha[2]FCP **2** (singlet at δ 20.43 ppm), ferrocene substituted cyclic P_4-species **3** (singlet at δ 39.10 ppm) and ^{t}Bu-substituted linear P_4-species **7** (multiplets at δ −41.63 and 3.57 ppm). The identity of by-products **2**, **3** and **7** indicates successful P–C bond activation with elimination of the alkyl unit at phosphorus, as intended.

Removal of the low molecular by-products from the product mixture *via* repeated extraction with toluene and pentane, followed by drying under reduced pressure (10^{-3} mbar), affords the actual product **6** as an intractable solid which was characterized with solid-state NMR, IR spectroscopy and elemental analysis.

For identification of structural units in compound **6**, solid-state NMR measurements have been performed. The $^1H \rightarrow {}^{31}P$ CP MAS NMR spectrum of **6** (Fig. 3B) shows a pattern of few broad ^{31}P resonances centered at around δ −8, −20 and −26 ppm reminiscent of those observed for closely related polymers **4** and **5**, which have been prepared from strained

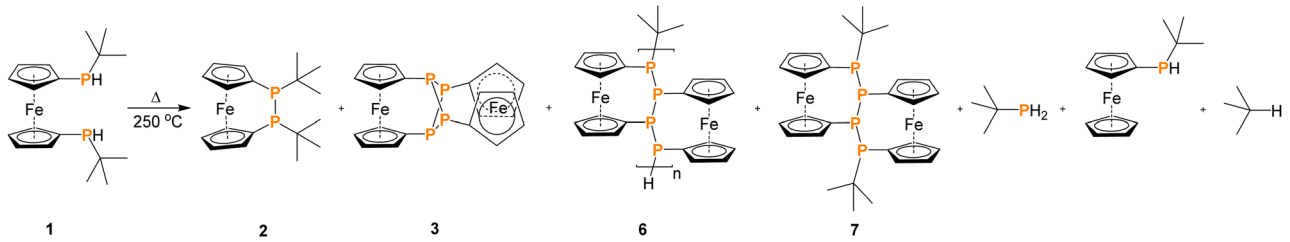

Scheme 3 Thermal reactions of **1**.

precursors.[13,15,18] For detailed comparison of polymer **6** with the previously reported analogous polymer **5**, an authentic sample of **5** was characterized with $^{1}H \rightarrow {}^{31}P$ CP MAS NMR spectroscopy under otherwise identical conditions (Fig. 3A). By direct comparison, the $^{1}H \rightarrow {}^{31}P$ CP MAS NMR signatures of **5** and **6** match closely and are consistent with chemically equivalent phosphorus centres in the backbone. It is also noteworthy that the above mentioned ^{31}P resonances at δ −8, −20 and −26 ppm for **5** and **6** are in good agreement with solid-state NMR data obtained for *o*-phenylene bridged (macro)cyclic cyclopolyphosphanes, reported by Woollins *et al.* (δ (^{31}P) = −21.8 ppm),[34] and for **4**, reported by us (^{31}P δ −10 (Cp*P*(^{t}Bu)P) and −24 ppm (Cp*P*(P)$_2$).[13] While related short chain oligomers in solution feature well resolved higher order spin systems, the *J*-couplings are not resolved in the above mentioned solid-state NMR spectra, as expected.

To overcome the limitations imposed by line broadening and to analyze scalar couplings in the solid-state, we also measured ^{31}P *J*-resolved solid state ^{31}P NMR spectra of **5** and **6**. As a result, ^{31}P–^{31}P couplings with *ca.* 290 Hz were observed in both cases for the main signals resonating at δ −8, −20 and −26 ppm (Fig. 3C and D). Further couplings in the order of 140 and 550 Hz are detectable for the signal appearing at *ca.* δ −8 −20 and −26 ppm, for polymers **5** and **6**, respectively. Clearly, scalar couplings reflect the s-character of the respective bond path and are strongly dependent on the angular geometry. It is here noteworthy that these couplings are smaller or larger than those found for the phosphanes in the *trans*-position of the Wilkinson's catalyst, featuring a value of *ca.* 394 Hz in the solid state. (Fig. S13, SI).[35] For the sake of completeness, the stereogenic nature of the phosphorus atoms needs to be considered leading to complex diastereomeric mixtures in the case of open chain 1D-polyphosphanes.[36] However, coplanar arrangement of the polyphosphane chain has been demonstrated for **4** further corroborated by single crystal XRD for short chain oligomers such as **7**. Owing to the presence of a bisecting mirror plane along the phosphorus chain, the resulting achiral *meso*-form is likely to be the reason for the relatively simple signal pattern observed for **4**, **5** and **6**.

The subtle difference between these three polymers lies mainly in their terminal groups, with **4** featuring two *tert*-butyl groups as terminal groups, **5** being a closed loop without terminal groups, and **6** carrying either *tert*-butyl or H at the terminal positions. One might speculate that the partial H-termination in **6** is a result of the presence of the P–H unit in the precursor rather than of isobutene elimination from a P–^{t}Bu unit, since otherwise polymer **4** would contain P–H units as well, which is not the case. Owing to the low reactivity of the solvents used in the extraction of by-products, alteration of these functionalities during the purification process is highly unlikely.

To probe the presence of H atoms on terminal P-atoms, ^{31}P sostapt (solid state attached proton test) NMR experiments in the solid state were performed for polymer **6**. The spectra (Fig. S18, SI) were recorded individually and consecutively with and without applying ^{1}H pulse power during inversion of ^{31}P with a 180° pulse. By switching all ^{31}P nuclei, other than those coupled directly to ^{1}H, the signal resulting from the P atom resonating at

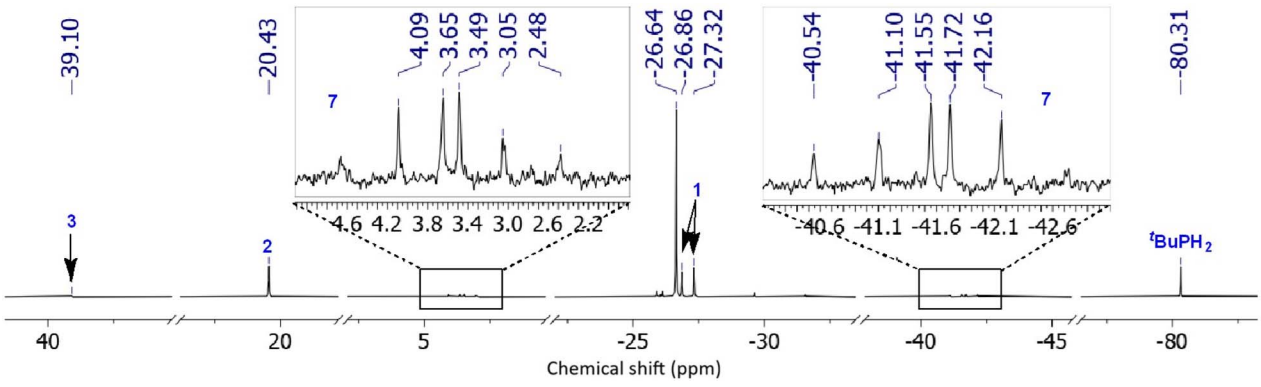

Fig. 2 ^{31}P (ref. 33) NMR (in C_6D_6) spectrum of the soluble product from thermal polymerization of **1**, where the singlet at δ −26.64 ppm results from Fc*P*^{t}BuH.

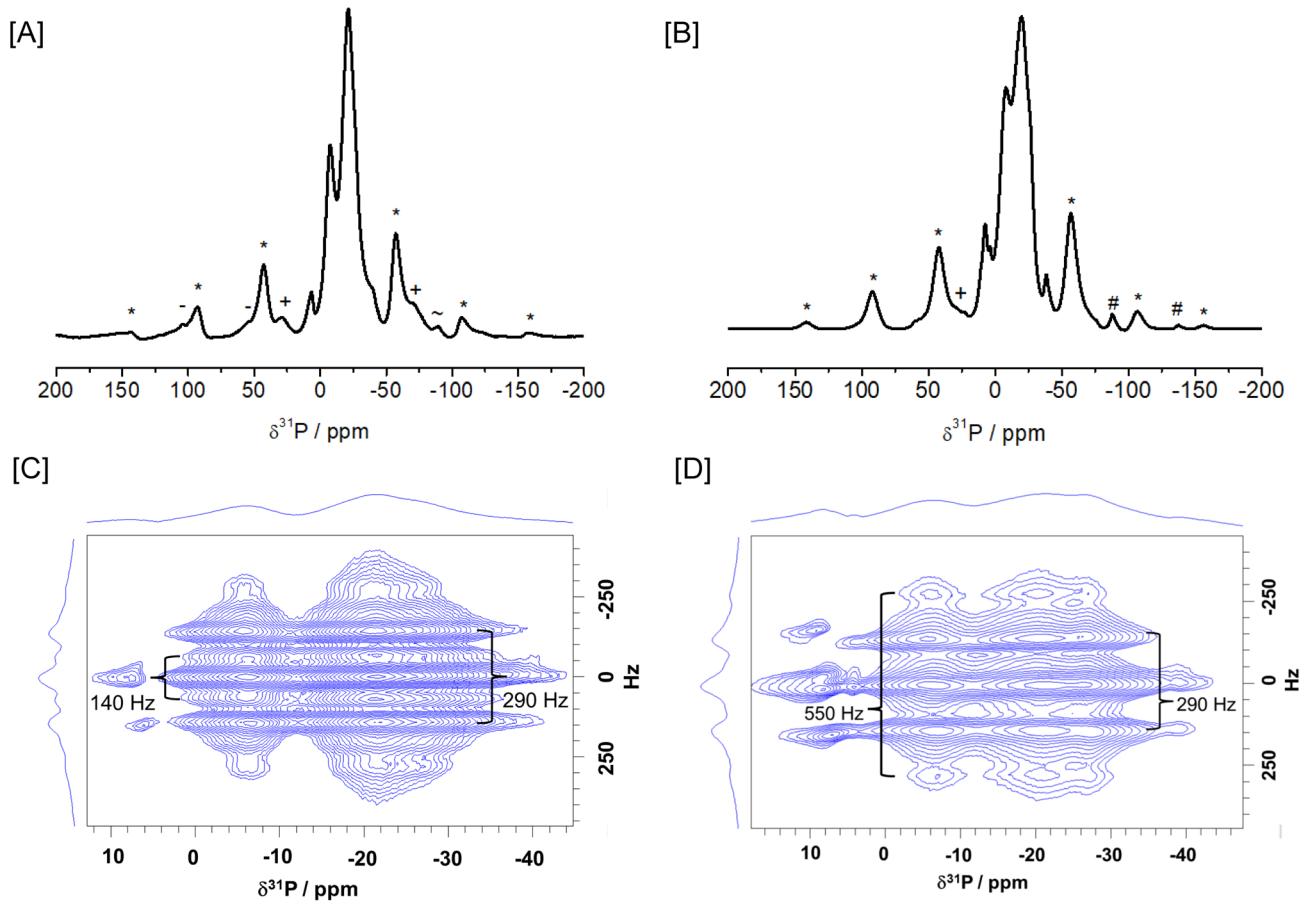

Fig. 3 $^{1}H \rightarrow {}^{31}P$ CP MAS NMR spectra (measured at 14 T and 12 kHz spinning) of **5** (A) and **6** (B) with spinning sidebands marked with asterisks, plus, minus or tilde; ^{31}P *J*-resolved NMR spectra (featuring ^{31}P–^{31}P couplings) of **5** (C) and **6** (D).

about δ −26.5 ppm shows negative amplitude, indicative of H-containing terminal P atoms. These interpretations are further consistent with the $^{1}H \rightarrow {}^{13}C$ CP MAS NMR spectrum of **6** featuring a weak intensity signal at δ *ca.* 31 ppm, which can be assigned to residual *tert*-butyl as part of the end group (Fig. S14, SI). Unfortunately, the distortion of the signal intensity encountered during $^{1}H \rightarrow X$ cross polarization precludes signal integration to quantify the abundance of the structural units. To get independent information on the ratio of the end group *vs.* main chain units in **6**, CHN elemental analyses from two independently synthesized samples have been performed. Using average values over several samples in each case, best agreement has been obtained by assuming two distinct compositions of *ca.* ^{t}Bu–$[Fe(C_5H_4P)_2]_{86–95}$–H and ^{t}Bu–$[Fe(C_5H_4P)_2]_{608–2536}$–H, indicating slightly and moderately longer chain length, as compared to **4**.[13] Compound **6** is stable and does not show any significant change upon further heating up to *ca.* 400 °C, as confirmed by elemental analysis. The constitutional similarity of **4**, **5** and **6** was further corroborated by vibrational spectroscopy, where comparison of the IR spectra of **4**,[13] **5**,[15] and **6** (Fig. S19, SI), in all cases, shows three strong signals and one medium strong signal in the range of ν 810–815 cm^{-1}, 1022–1025 cm^{-1}, and 1152–1158 cm^{-1} for out of plane C^{Cp}–H bending, ring breathing, and asymmetric ring breathing of C^{Cp}–C^{Cp}, respectively in order.[37,38] Stretching vibrations for the Cp–P bond are generally observed in the region of 1000–1100 cm^{-1}, often overlapping with the Cp ring breathing modes.[39] In order to explore the electronic excitation of these polymeric materials, UV-vis measurements were performed. In contrast to the parent ferrocene, which is known to exhibit two distinct absorption bands in the visible range, at 322 nm with a very low intensity and at 442 nm with high intensity,[40] polymers **4**, **5** and **6** feature much broader absorption bands in the solid state with almost equal intensities for the two previously mentioned absorptions (Fig. 4). Moreover, the band at *ca.* 440 nm shows an intense shoulder at above 500 nm which is more red shifted and intense for **5** and **6** than for **4**. In addition, these absorptions tail off still having significant intensities at wavelengths above 600 nm which are most pronounced for **6** followed by **5** and **4**. For the parent ferrocene, the bands at 440 nm with a weak shoulder at 528 nm have been assigned to dipole forbidden transitions which gain oscillator strength *via* vibronic coupling.[41] In line with this, in substituted ferrocenes the intensity of the latter increases and is shifted to longer wavelengths.[40] In the same vein, the higher energy transition at 322 nm has been reported to gain intensity upon mono- or di-substitution at ferrocene's Cp-rings but to lose intensity upon further substitution. In line with these findings, the high intensities and red shifted absorptions of **4**, **5** and **6** in the high energy

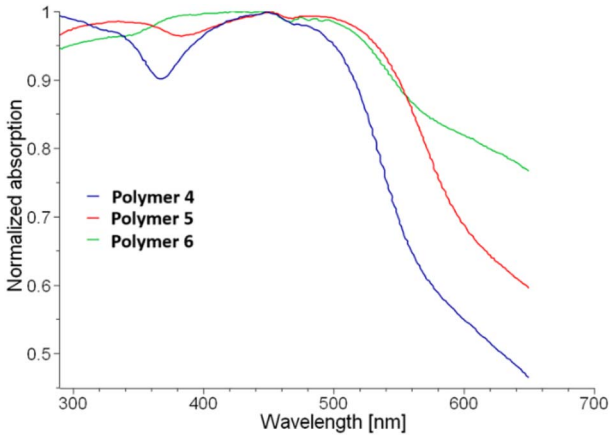

Fig. 4 Solid state UV-vis spectra of polymers **4**, **5** and **6**.

region at *ca.* 325 nm are consistent with electronic modification of the Cp-ligands. The remarkable intensity gain for the absorption shoulder at above 500 nm for **4**, **5** and **6** most likely is a consequence of vibronic coupling as previously mentioned. To gain insight into this phenomenon, we performed DFT calculations on oligomeric model systems. Investigation of the frontier molecular orbitals indicates significant interaction of the lone pairs at phosphorus in the ferrocenylene bridged all-*trans* oriented phosphorus chain (Fig. S25). In consequence, the HOMO–LUMO gap significantly decreases in agreement with the observed red-shifted absorption in the UV-vis region outlined above. The observed red-shifted absorption maxima and the spectral tail extending into the visible region are in agreement with the TD-DFT calculations on the model oligomeric system, which indicate several excited states with low oscillator strength above 450 nm. It needs to be noted that the pronounced absorption features at long wavelengths are significantly red-shifted compared with saturated low-molecular phosphanylferrocenes, such as compound **1**, for which the solid-state UV-vis absorption spectrum was measured under identical conditions for comparison (Fig. S26). Interestingly, the absorption of **4**, **5** and **6** above 500 nm already comes close to the absorption wavelength reported for related unsaturated phosphanylferrocenes containing diphosphene units located at *ca.* 540 nm.[42–46]

To further understand the relevance of the P–H bond in the thermal conversion of **1** to **6**, we treated an analog in which the P–H unit is replaced by a second *tert*-butyl group, namely Fc′(P^tBu_2)$_2$ under identical conditions in a sealed ampule at 250 °C. However, to our surprise, the reaction proceeded *via* an uncontrolled P–C bond cleavage, where phosphorus-free Fc(^{t}Bu) and ^{t}Bu–^{t}Bu were obtained as major products, along with Fc^{i}Pr, 1,1′-Fc′(^{t}Bu)$_2$, and 1,3,1′-Fc′(^{t}Bu)$_3$, in trace amounts (Scheme 4; Fig. S23 and S24, SI). This result has further been corroborated with MALDI MS, whereas no notable polymeric material could be recovered from this reaction. Moreover, the phosphorus content has been entirely transferred to the volatile by-products indicating a preferred cleavage of the P–C bond to the ferrocene in this particular case.

In order to understand the reactivity of the two different systems, DFT calculations were performed. Several possible reaction pathways, intermediates, and side products were considered (more details in the SI). In view of the harsh reaction conditions, homolytic P–C bond cleavage is proposed as the initial step (Schemes S1 and S3, SI). The cleavage of the P–C(^{t}Bu) bond is less hindered (ΔG = 46 kcal mol^{-1} for **1** and ΔG = 38 kcal mol^{-1} for **8**, Scheme S1, SI) in both cases than the respective cleavage between the ferrocene unit and the phosphorus moiety (ΔG = 77 kcal mol^{-1} for **1** and ΔG = 69 kcal mol^{-1} for **8**, Scheme S2, SI). Although both P–C(^{t}Bu) and P–Cp cleavages are favorable for **8**, the observed reaction pathways contrasted our theoretical findings. Furthermore, considering the possible subsequent reactions, no significant differences in Gibbs free energy were observed among the pathways (Scheme S3), suggesting that the presence of the two *tert*-butyl groups may influence the reaction in other unprecedented ways. A possible explanation could be the availability of the eclipsed geometry, promoting intramolecular radical transfer and the formation of P–P-bonded products. In the case of **8**, the eclipsed geometry is likely less favourable, allowing alternative reaction pathways to dominate. The considered reaction paths (Scheme 5) result in the formation of volatile phosphorus-containing by-products (*e.g.* PH_3), which is consistent with the experiments, as no phosphorus-containing solid products were spectroscopically found when starting from precursor **8**.

Comparing the overall synthetic strategies to such metallopolymers, it needs to be pointed out that using compound **1** as the direct precursor as reported here is significantly more efficient and atom-economic than the previously published approach to **4**, where the actual precursor **2** likewise needs to be prepared from **1** in a multistep reaction involving metalation with *n*-butyl lithium and oxidative coupling to [2]ferrocenophane **2**. Therefore, these latter additional steps can be saved by using **1** as a direct precursor to **6**. Otherwise, the energy

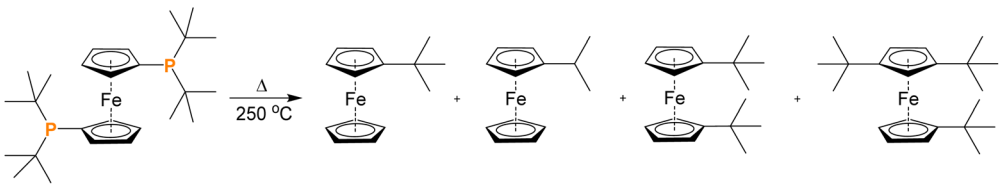

Scheme 4 Thermal reactions of Fc′(P^tBu_2)$_2$.

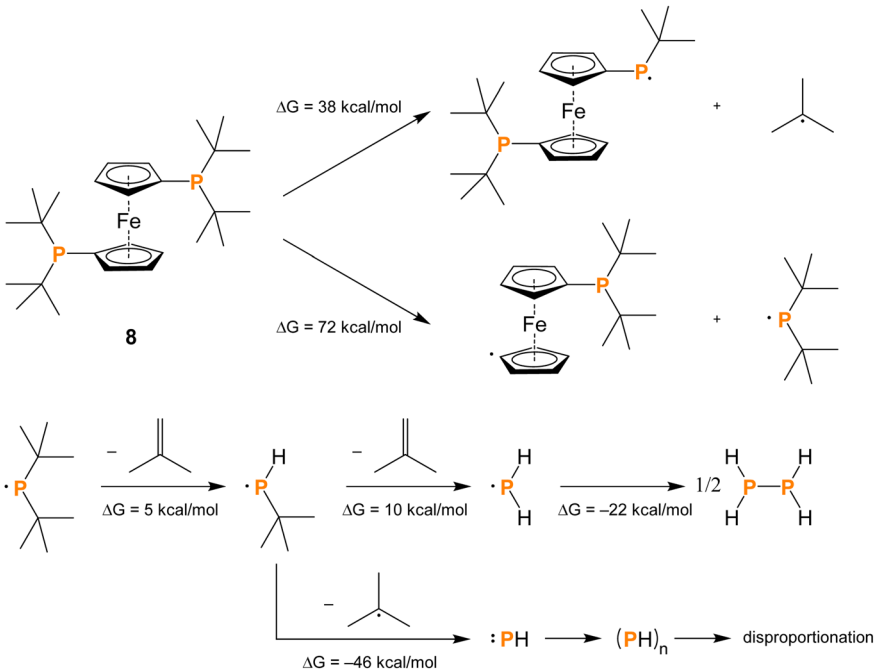

Scheme 5 Thermodynamic profile of the thermal decomposition pathways of Fc′(P^tBu_2)$_2$ and its fragments computed at the ωB97X-D/6-311 + g** level of theory.

requirements, reaction times and yields are almost identical in the thermolytic reactions to **4** and **6**.

3. Experimental

3.1. General methodology

All manipulations were performed under an argon atmosphere unless mentioned otherwise. Prior to use, the glassware was dried in a drying oven at 120 °C. Solvents were distilled over drying agents, prescribed in the CRC Handbook of Chemistry and subsequently stored under an argon atmosphere over 4 Å molecular sieves. Solvents for column chromatography and aqueous workups were used (analytical grade was supplied by VWR and Alfa-Aesar) without further purification. NMR solvents (purchased from Deutero) were degassed *via* a few cycles of freeze, pump and thaw and finally stored over 3 Å molecular sieves under an argon atmosphere. Reagents and chemicals were purchased from commercial suppliers (Sigma-Aldrich, ABCR, and Alfa-Aesar) and used as received. Fc′(P^tBuH)$_2$ and polymers **4** and **5** were synthesized by following a published procedure.[13,15,31]

All solution-phase NMR spectra were measured on Jeol JNM-ECZL500, Varian 500VNMRS and Varian MR-400 spectrometers at 25 °C. Chemical shifts were referenced to residual protic impurities in the solvent (^{1}H) or the deuterated solvent (^{13}C) and reported relative to external $SiMe_4$ (^{1}H, ^{13}C). The signals, resulting from the residual nondeuterated NMR solvents, were referenced as indicated in the literature.[47] NMR spectra of heteronuclei were referenced using the Ξ-scale following IUPAC recommendations with H_3PO_4 (85%) (^{31}P) as the secondary reference.[48]

All solid-state NMR measurements were performed on a Bruker Avance III HD 600 MHz spectrometer employing a 4 mm broad band H/X probe. Samples were packed into ZrO_2 rotors. All spectra were recorded at 14 T, which leads to frequencies of 150.92 MHz for ^{13}C, 242.93 MHz for ^{31}P and 600.12 MHz for ^{1}H respectively, at room temperature with a MAS spinning frequency of 8, 10 or 12 kHz as indicated in the figure captions. The CP MAS sequence was used with a linear 50–100 ramp on ^{1}H and a contact time of 3.5 ms for ^{31}P and 2 ms for ^{13}C. A π/2 excitation pulse of 2.5 μs was applied on ^{1}H. TPPM15 broadband decoupling was applied during data acquisition.[49,50] A recycle delay of 1 or 3 s, respectively, was used for all spectra. ^{31}P spectra were recorded with 1024 and 256 scans and ^{13}C spectra with 2028 scans, respectively. As a reference, H_3PO_4 (0 ppm) was used for ^{31}P, and TMS (0 ppm) was used for ^{13}C. ^{31}P *J*-resolved spectra were recorded to establish ^{31}P polarization by means of CP with the parameters described above.[35] This was followed by a rotor synchronized π pulse (n = 1, 2, …) of 5 μs on ^{31}P and recording the spin echo. The ^{31}P sostapt experiments were recorded at 12 kHz spinning employing the pulse sequence introduced by Lesage *et al.*[51] which is implemented in the Bruker Topspin 3.2 software package. Parameters for CP were used as described above. The π pulses were set to 5 μs in the sequence. Homonuclear ^{1}H–^{1}H decoupling during the evolution time τ was performed by employing frequency switched Lee-Goldburg (FSLG).[52]

MALDI measurements were performed with Ultraflex der Firma Bruker Daltonics instruments using samples dissolved in HPLC-quality solvents. Elemental analyses were performed without using any external oxidizer on an EA 3000 Elemental Analyzer (EuroVector). Infrared spectra recorded for the neat

substances were obtained using a Bruker Alpha Platinum ATR spectrometer, and Opus 6.5 (from Bruker Optics) was used for analysing the data. Strong, medium strong and weak peaks for these species were denoted as s, m and w, respectively. UV-vis spectra were measured with a Hamamatsu C11347 system in solid state and for the refinement of data, OriginPro was used.

3.2. Solid-state NMR characterization of polymer 5

Polymer **5** was synthesized by following a previously published procedure.[15] $^{1}H \rightarrow {}^{13}C$ CP MAS NMR δ [ppm]: 79 and 73 (C^{Cp}) (Fig. S8, SI). $^{1}H \rightarrow {}^{31}P$ CP MAS NMR δ [ppm]: 8, −8, −20 and −38 ppm (Fig. S9 and S10, SI).

3.3. Thermal oligo- and polymerization of 1 and synthesis of 6

100 mg of compound **1** was taken in a glass-vial and sealed under a vacuum of 10^{-3} mbar, before keeping it at 250 °C for 4 h. After cooling the vials down at room temperature, the inner soluble substances were dissolved in C_6D_6. ^{1}H NMR (C_6D_6) δ [ppm]: 0.87 (d, $(CH_3)_3CH$, $J = 7$ Hz from Me_3CH), and 1.63 (dh, $(CH_3)_3CH$, $J = 13$, 7 Hz from Me_3CH) (Fig. S1, ESI). ^{13}C NMR (C_6D_6) δ [ppm]: 24.78 (s, $(CH_3)_3CH$ from Me_3CH) (Fig. S2, ESI). ^{31}P NMR (C_6D_6) δ [ppm]: 39.09 (s, Fc′$_2P_2$ from **3**), 20.43 (bm, (^{t}BuP)$_2$[2]FCP from **2**), 3.60 (m, ^{t}Bu*P*-P from **7**), −26.12 (ddq, $J =$ 206, 24, 12 Hz from Fc′(P^tBuH)$_2$), −27.14 (d, $J = 207$ Hz from FcP^tBuH), −41.36 (m, ^{t}BuP-*P* from **7**), and −80.29 (dddd, $J =$ 198.5, 174.9, 23.7, 11.8 Hz from ^{t}Bu*P*H$_2$) (Fig. S3, ESI). $^{31}P\{^1H\}$ NMR (C_6D_6) δ [ppm]: 39.10 (s, Fc′$_2P_2$ from **3**), 20.43 (s, (^{t}BuP)$_2$[2] FCP from **2**), 3.57 (m, ^{t}Bu*P*-P from **7**), −26.64 (s from FcP^tBuH), −27.08 (d, $J = 94$ Hz from **1**), −41.64 (m, ^{t}BuP-*P* from **7**), and −80.31 (s from ^{t}Bu*P*H$_2$) (Fig. 2). Molecular ion peaks for compounds **2**, **3**, and **7** have appeared at *m*/*z* 360.185 (calcd. value 360.199), 491.931 (calcd. value 491.933), and 606.049 (calcd. value 606.165), respectively (Fig. S5–S7, SI).

After washing all the soluble materials with toluene (3 × 10 ml) and pentane (3 × 10 ml), the residual solid materials (**6**) were kept under 10^{-3} mbar vacuum, before characterizing *via* solid-state NMR measurements. ^{13}C NMR (solid-state) δ [ppm]: 79 and 73 (C^{Cp}), 31 (^{t}Bu) (Fig. S14, SI). ^{31}P NMR (solid-state) δ [ppm]: 8, −8, −20 and −38 ppm (Fig. S15 and S16, SI). Anal. Calcd. for $[C_{10}H_8FeP_2]_n$ (neglecting the terminal groups): C, 48.83; H, 3.28. Found: C, 48.92; H, 3.31 and C, 48.84; H, 3.28 for two parallelly performed identical polymerization reactions. Closer inspection taking terminal *tert*-butyl and H end groups into account indicates the molecular formula as $[C_4H_9]$–$[C_{10}H_8FeP_2]_{86-95}$ H (where $C_4H_9 = {}^t$Bu) from the first reaction, based on the average of samples from four consecutively measured elemental compositions: C, 48.92; H, 3.31 (SD 0.07, SEM 0.02), where anal. calcd. For $[C_4H_9]$–$[C_{10}H_8FeP_2]_{86-95}$–H: C, 48.92; H, 3.31. On the other hand, the molecular formula could be found as $[C_4H_9]$–$[C_{10}H_8FeP_2]_{608-2536}$–H from the second reaction, based on the average of samples from four consecutively measured elemental compositions: C, 48.84; H, 3.28 (SD 0.03, SEM 0.04), where Anal. Calcd. For $[C_{10}H_8FeP_2]_{86-95}[C_4H_9]$ H: C, 48.84; H, 3.28. IR (ATR) ν: 810 (s, out of plane C^{Cp}–H bend), 848 (m, out of plane C^{Cp}–C^{Cp} bend), 892 (m, out of plane C^{Cp}–C^{Cp} bend), 1024 (s, ring breathing), 1157 (s, asymmetric ring breathing), 1363, (w, in-plane skeletal C^{Cp}–C^{Cp} vibration), and 1387 (m, in-plane skeletal C^{Cp}–C^{Cp} vibration) (Fig. S19, SI).

3.4. Thermal oligo- and polymerization of Fc′(P^tBu$_2$)$_2$

100 mg of compound Fc′(P^tBu$_2$)$_2$ was taken in a glass-vial and sealed under a vacuum of 10^{-3} mbar, before keeping it at 250 °C for 4 h. The crude product was dissolved in C_6D_6 before characterization with various methods. ^{1}H NMR (C_6D_6) δ [ppm]: 0.87 (d, $J = 7$ Hz, Fc-C(CH_3)$_3$ of Fc(^{t}Bu)), 1.20 (s, (CH_3)$_3$C– C(CH_3)$_3$), 3.92 (pst, β-H of Cp$^{t\mathrm{Bu}}$ of Fc(^{t}Bu)), 3.96 (pst, α-H of Cp$^{t\mathrm{Bu}}$ of Fc(^{t}Bu)), 4.01 (ferrocene) and 4.04 (s, C_5H_5 of Fc(^{t}Bu)) (Fig. S20, SI). ^{13}C NMR (C_6D_6) δ [ppm]: 24.79 (s, (CH_3)$_3$C– C(CH_3)$_3$), 31.59 (s, Fc-C(CH_3)$_3$ of Fc(^{t}Bu)), 65.26 (s, β-C of Cp$^{t\mathrm{Bu}}$ of Fc(^{t}Bu)), 67.22 (s, α-C of Cp$^{t\mathrm{Bu}}$ of Fc(^{t}Bu)), 68.23 (ferrocene), and 68.46 (s, C_5H_5 of Fc(^{t}Bu)) (Fig. S21, SI). Molecular ion peaks for compounds Fc^{i}Pr, Fc(^{t}Bu), 1,1′-Fc′(^{t}Bu)$_2$, and 1,3,1′-Fc′(^{t}Bu)$_3$ have appeared at *m*/*z* 227.052 (M–1 calcd. value 227.116), 242.075 (calcd. value 242.143), 298.137 (calcd. value 298.251), 354.200 (calcd. value 354.359), respectively (Fig. S23, ESI). MALDI (HRMS) for Fc(^{t}Bu): *m*/*z* 242.0752 (calcd. value 242.0758) (Fig. S23 and S24, SI). NOTE: the empty baseline in $^{31}P\{^1H\}$ NMR signifies the absence of any soluble P-containing species in the reaction mixture (Fig. S22, SI).

4. Theoretical calculations

All calculations were performed using the Gaussian 16 program package,[53] and Molden[54] was used to visualize the computed structures. Geometry optimizations were carried out at the ωB97X-D/6-311+G** level of theory. In some cases, the results were further validated by LNO-CCSD(T)/def2-TZVP single-point calculations performed with the MRCC program package.[55,56] Harmonic vibrational frequency analyses were performed on the fully optimized structures to verify their character; minima were confirmed by the presence of exclusively positive Hessian eigenvalues. Gibbs free energies were calculated at 298.15 K and atmospheric pressure using the computed harmonic frequencies.

5. Conclusions

In summary, we explored the question of whether unstrained open-chain 1,1′-diphosphaferrocenes are capable of undergoing thermal dealkylation to metallopolymers or whether the ring strain of cyclic precursors currently in use is required. We found that comparable metallopolymers are accessible from unstrained open-chain precursors, but the substitution pattern decisively controls the product formation. Further indications for this reactivity were found in a multi-step reaction mechanism elucidated using DFT calculations, where the initial step is homolytic P–H and P–C(^{t}Bu) cleavages, forming dehydrogenated and dealkylated intermediates [(η^5-C_5H_4-P^{t}Bu)Fe(η^5-C_5H_4-PH^{t}Bu)]$^\bullet$ and [(η^5-C_5H_4-PH)Fe(η^5-C_5H_4–P(^{t}Bu$_2$)]$^\bullet$ from **1** and **8**, respectively. Due to the steric congestion between *tert*-butyl groups, species [(η^5-C_5H_4-P^{t}Bu)Fe(η^5-C_5H_4-PH(^{t}Bu$_2$)]$^\bullet$ does not support eclipsed orientation on the ferrocene moiety

and consequently undergoes further thermal cleavages of P–C(^{t}Bu), followed by those of P-Cp bonds, giving rise to Fc(^{t}Bu) as an identifiable major product with minor and trace impurities of other mono-, di-, and tri-substituted ferrocenes. Solid state ^{1}H → ^{31}P CP MAS NMR turned out to be the most valuable technique for characterization of the polymer backbone *via* comparison of its characteristic NMR signature with those of closely related polymers. Indications for P–H termination have been obtained using ^{31}P sostapt NMR experiments in the solid state. However, cross polarization precludes quantitative information on the relative abundance of structural units. Obviously, simple and robust precursors, such as **1** which is air stable as a neat substance,[32] will facilitate the accessibility of metallopolymers. Its direct use as a precursor to metallopolymers avoids additional synthetic effort in preparing strained precursors from the same starting compound. We are convinced that further examples of unstrained precursors with reactive element-carbon bonds will lead to their respective metallopolymers in the future.

Ulrich Schubert dedication

The authors dedicate this work to Professor Dr Ulrich Schubert on the occasion of his 80th birthday in recognition of his exceptional scientific achievements and enduring impact in materials chemistry.

Author contributions

Subhayan Dey: investigation and conceptualization; Balázs Szathmári: investigation; Dennis Langgut: investigation; Zsolt Kelemen: supervision and conceptualization; Torsten Gutmann: supervision and conceptualization; Rudolf Pietschnig: supervision and conceptualization.

Conflicts of interest

The authors declare no conflict of interest.

Data availability

The supporting data have been provided as part of the supplementary information (SI). Supplementary information: Fig. S1–S26, NMR spectra, MS spectra, IR spectra, UV/vis spectra, and Kohn–Sham FMO; Schemes S1–S5, computational information on thermodynamic decomposition pathways. Geometries of computed structures have been provided as an *xyz*-file. See DOI: https://doi.org/10.1039/d6ta02261h.

Acknowledgements

S. D. thanks the Vellore Institute of Technology, Chennai Campus, India, for providing the "VIT RGEMS SEED GRANT" (Sanction Order No. PH1/2024/SG2024001) for carrying out this research work. We thank Prof. Buntkowsky (TU Darmstadt) for generous allocation of measurement time slots on his 600 MHz Bruker Avance III HD spectrometer. Dr Hergen Breitzke is gratefully acknowledged for technical support of the solid-state NMR measurements. R. P. and S. D. are further grateful to the University of Kassel ZFF-program for their generous contribution in funding this research. Z. K. is grateful for the support of OTKA-FK-145841 provided by the National Research Development and Innovation Office of Hungary.

References

1 J. E. Mark, H. R. Allcock and R. West, *Inorganic Polymers*, Prentice Hall, NJ, USA, 1992.
2 V. Chandrasekhar, *Inorganic and Organometallic Polymers*, Springer Berlin Heidelberg, Germany, 2005.
3 B. Toury and P. Miele, *J. Mater. Chem.*, 2004, **14**, 2609–2611.
4 R. Pietschnig, *Chem. Soc. Rev.*, 2016, **45**, 5216–5231.
5 V. Bellas and M. Rehahn, *Angew. Chem., Int. Ed.*, 2007, **46**, 5082–5104.
6 D. Löber, S. Dey, B. Kaban, F. Roesler, M. Maurer, H. Hillmer and R. Pietschnig, *Molecules*, 2020, **25**, 2438.
7 S. Vijayalakshmi, S. Dey and K. Rajendrakumar, *J. Macromol. Sci. Part A Pure Appl. Chem.*, 2025, **63**, 1–18.
8 D. E. Herbert, U. F. Mayer and I. Manners, *Angew. Chem., Int. Ed.*, 2007, **46**, 5060–5081.
9 H. Bhattacharjee, S. Dey, J. Zhu, W. Sun and J. Muller, *Chem. Commun.*, 2018, **54**, 5562–5565.
10 E. Khozeimeh Sarbisheh, H. Bhattacharjee, M. P. T. Cao, J. Zhu and J. Müller, *Organometallics*, 2017, **36**, 614–621.
11 H. P. Withers, D. Seyferth, J. D. Fellmann, P. E. Garrou and S. Martin, *Organometallics*, 1982, **1**, 1283–1288.
12 R. Rulkens, A. J. Lough and I. Manners, *J. Am. Chem. Soc.*, 1994, **116**, 797–798.
13 S. Dey, D. Kargin, M. V. Höfler, B. Szathmári, C. Bruhn, T. Gutmann, Z. Kelemen and R. Pietschnig, *Polymer*, 2022, **242**, 124589.
14 Y. Tanimoto, Y. Ishizu, K. Kubo, K. Miyoshi and T. Mizuta, *J. Organomet. Chem.*, 2012, **713**, 80–88.
15 S. Dey, B. Szathmari, R. Franz, C. Bruhn, Z. Kelemen and R. Pietschnig, *Chem.–Eur. J.*, 2024, **30**, e202400194.
16 C. T. Aitken, J. F. Harrod and E. Samuel, *J. Am. Chem. Soc.*, 1986, **108**, 4059–4066.
17 S. M. Katz, J. A. Reichl and D. H. Berry, *J. Am. Chem. Soc.*, 1998, **120**, 9844–9849.
18 T. Imori, V. Lu, H. Cai and T. D. Tilley, *J. Am. Chem. Soc.*, 1995, **117**, 9931–9940.
19 H. Dorn, J. M. Rodezno, B. Brunnhöfer, E. Rivard, J. A. Massey and I. Manners, *Macromolecules*, 2003, **36**, 291–297.
20 R. Zhang, J. E. Mark and A. R. Pinhas, *Macromolecules*, 2000, **33**, 3508–3510.
21 M. B. Reuter, D. M. Seth, D. R. Javier-Jiménez, E. J. Finfer, E. A. Beretta and R. Waterman, *Chem. Commun.*, 2023, **59**, 1258–1273.
22 R. J. Less, R. L. Melen and D. S. Wright, *RSC Adv.*, 2012, **2**, 2191–2199.
23 R. L. Melen, *Dalton Trans.*, 2013, **42**, 16449–16465.

24 W. J. Transue, A. Velian, M. Nava, C. García-Iriepa, M. Temprado and C. C. Cummins, *J. Am. Chem. Soc.*, 2017, **139**, 10822–10831.
25 V. Naseri, R. J. Less, R. E. Mulvey, M. McPartlin and D. S. Wright, *Chem. Commun.*, 2010, **46**, 5000–5002.
26 H. Schneider, D. Schmidt and U. Radius, *Chem. Commun.*, 2015, **51**, 10138–10141.
27 V. J. Eilrich and E. Hey-Hawkins, *Coord. Chem. Rev.*, 2021, **437**, 213749.
28 T. N. Hooper, A. S. Weller, N. A. Beattie and S. A. Macgregor, *Chem. Sci.*, 2016, **7**, 2414–2426.
29 D. Han, F. Anke, M. Trose and T. Beweries, *Coord. Chem. Rev.*, 2019, **380**, 260–286.
30 A. Schäfer, T. Jurca, J. Turner, J. R. Vance, K. Lee, V. A. Du, M. F. Haddow, G. R. Whittell and I. Manners, *Angew. Chem., Int. Ed.*, 2015, **54**, 4836–4841.
31 D. Kargin, Z. Kelemen, K. Krekic, M. Maurer, C. Bruhn, L. Nyulaszi and R. Pietschnig, *Dalton Trans.*, 2016, **45**, 2180–2189.
32 F. Horký, R. Franz, C. Bruhn and R. Pietschnig, *Chem.–Eur. J.*, 2023, **29**, e202302518.
33 K. P. Barry and C. Nataro, *Inorg. Chim. Acta*, 2009, **362**, 2068–2070.
34 P. Kilian, A. M. Z. Slawin and J. D. Woollins, *Chem.–Eur. J.*, 2003, **9**, 215–222.
35 A. Grünberg, X. Yeping, H. Breitzke and G. Buntkowsky, *Chem.–Eur. J.*, 2010, **16**, 6993–6998.
36 R. Wolf, M. Finger, C. Limburg, A. C. Willis, S. B. Wild and E. Hey-Hawkins, *Dalton Trans.*, 2006, 831–837.
37 L. Phillips, A. R. Lacey and M. K. Cooper, *J. Chem. Soc., Dalton Trans.*, 1988, 1383–1391.
38 T. P. Gerasimova and S. A. Katsyuba, *J. Organomet. Chem.*, 2015, **776**, 30–34.
39 V. Ivanovski, M. Bukleski, M. Madalska and E. Hey-Hawkins, *Vib. Spectrosc.*, 2013, **69**, 57–64.
40 A. Paul, R. Borrelli, H. Bouyanfif, S. Gottis and F. Sauvage, *ACS Omega*, 2019, **4**, 14780–14789.
41 U. Salzner, *J. Chem. Theory Comput.*, 2013, **9**, 4064–4073.
42 R. Pietschnig and E. Niecke, *Organometallics*, 1996, **15**, 891–893.
43 N. Nagahora, T. Sasamori, N. Takeda and N. Tokitoh, *Chem.–Eur. J.*, 2004, **10**, 6146–6151.
44 C. Moser, M. Nieger and R. Pietschnig, *Organometallics*, 2006, **25**, 2667–2672.
45 N. Nagahora, T. Sasamori, Y. Watanabe, Y. Furukawa and N. Tokitoh, *Bull. Chem. Soc. Jpn.*, 2007, **80**, 1884–1900.
46 T. Sasamori, M. Sakagami, M. Niwa, H. Sakai, Y. Furukawa and N. Tokitoh, *Chem. Commun.*, 2012, **48**, 8562–8564.
47 G. R. Fulmer, A. J. M. Miller, N. H. Sherden, H. E. Gottlieb, A. Nudelman, B. M. Stoltz, J. E. Bercaw and K. I. Goldberg, *Organometallics*, 2010, **29**, 2176–2179.
48 R. K. Harris, E. D. Becker, S. M. Cabral de Menezes, R. Goodfellow and P. Granger, *Pure Appl. Chem.*, 2001, **73**, 1795–1818.
49 I. Scholz, P. Hodgkinson, B. H. Meier and M. Ernst, *J. Chem. Phys.*, 2009, **130**, 114510.
50 S. Dey, F. Roesler, M. V. Höfler, C. Bruhn, T. Gutmann and R. Pietschnig, *Eur. J. Inorg. Chem.*, 2021, **2022**, e202100939.
51 A. Lesage, S. Steuernagel and L. Emsley, *J. Am. Chem. Soc.*, 1998, **120**, 7095–7100.
52 B. J. van Rossum, H. Förster and H. J. M. de Groot, *J. Magn. Reson.*, 1997, **124**, 516–519.
53 M. J. Frisch, G. W. Trucks, H. B. Schlegel, G. E. Scuseria, M. A. Robb, J. R. Cheeseman, G. Scalmani, V. Barone, G. A. Petersson, H. Nakatsuji, X. Li, M. Caricato, A. V. Marenich, J. Bloino, B. G. Janesko, R. Gomperts, B. Mennucci, H. P. Hratchian, J. V. Ortiz, A. F. Izmaylov, J. L. Sonnenberg, D. Williams-Young, F. Ding, F. Lipparini, F. Egidi, J. Goings, B. Peng, A. Petrone, T. Henderson, D. Ranasinghe, V. G. Zakrzewski, J. Gao, N. Rega, G. Zheng, W. Liang, M. Hada, M. Ehara, K. Toyota, R. Fukuda, J. Hasegawa, M. Ishida, T. Nakajima, Y. Honda, O. Kitao, H. Nakai, T. Vreven, K. Throssell, J. A. Montgomery Jr, J. E. Peralta, F. Ogliaro, M. J. Bearpark, J. J. Heyd, E. N. Brothers, K. N. Kudin, V. N. Staroverov, T. A. Keith, R. Kobayashi, J. Normand, K. Raghavachari, A. P. Rendell, J. C. Burant, S. S. Iyengar, J. Tomasi, M. Cossi, J. M. Millam, M. Klene, C. Adamo, R. Cammi, J. W. Ochterski, R. L. Martin, K. Morokuma, O. Farkas, J. B. Foresman and D. J. Fox, *Gaussian 16 Rev. C.01*, Wallingford, CT, 2016.
54 N. M. O'boyle, A. L. Tenderholt and K. M. Langner, *J. Comput. Chem.*, 2008, **29**, 839–845.
55 D. Mester, P. R. Nagy, J. Csóka, L. Gyevi-Nagy, P. B. Szabó, R. A. Horváth, K. Petrov, B. Hégely, B. Ladóczki, G. Samu, B. D. Lőrincz and M. Kállay, *J. Phys. Chem. A*, 2025, **129**, 2086–2107.
56 M. Kállay, P. R. Nagy, D. Mester, L. Gyevi-Nagy, J. Csóka, P. B. Szabó, Z. Rolik, G. Samu, B. Hégely, B. Ladóczki, K. Petrov, J. Csontos, Á. Ganyecz, I. Ladjánszki, L. Szegedy, M. Farkas, P. D. Mezei, R. A. Horváth and B. D. Lőrincz, *MRCC, a quantum chemical program suite*, https://www.mrcc.hu.